Materials Letters 338 (2023) 133999

Contents lists available at ScienceDirect

Materials Letters

journal homepage: www.elsevier.com/locate/matlet

Synthesis of carbonate hydroxyapatite contained magnesium cations by dry mechano-milling

Herlina Damayanti [a,b,*], Karlina Noordiningsih [b], Kristanto Wahyudi [b], Hernawan [b], Eneng Maryani [b], Anita Yuliati [c], Devi Rianti [c], Lia A.T.W. Asri [a,*], Rifki Septawendar [b]

[a] Materials Science and Engineering Research Group, Faculty of Mechanical and Aerospace Engineering, Institut Teknologi Bandung, Bandung 40132, Indonesia
[b] Center for Ceramics, Ministry of Industry of Indonesia Republic, Ahmad Yani 392, Bandung 40272, West Java, Indonesia
[c] Department of Dental Material, Faculty of Dental Medicine, Airlangga University, Mayjen Prof. Dr. Moestopo 47, Surabaya 60132, East Java, Indonesia

ARTICLE INFO

Keywords:
Carbonate hydroxyapatite
Dry mechano-milling
Magnesium carbonate
Hydroxyapatite
Biomaterial

ABSTRACT

The B-type carbonate hydroxyapatite (CHA) containing Mg cations was synthesized through the dry mechano-milling between Indonesian limestone-based hydroxyapatite (HA) and magnesium carbonate ($MgCO_3$). The novelty in this research is the selection of $MgCO_3$ as a precursor that will donate CO_3^{2-} and Mg^{2+} to the HA structure to form CHA-containing Mg cations. The crystalline phases and chemical structure of synthesized CHA were studied by X-ray diffraction, X-ray fluorescence, scanning electron microscope, and a particle size analyzer. The feasibility of this work is to be able to produce B-type CHA containing Mg cations that have the potential to be developed for biomaterial application.

1. Introduction

Carbonate hydroxyapatite (CHA) is an inorganic composition of natural apatite in the human bone that was classified into three types according to the substitutional site of incorporated CO_3^{2-} ions: A-type CHA (CO_3^{2-} substitutes OH^-), B-type CHA (CO_3^{2-} substitutes PO_4^{3-}), and AB-type CHA (CO_3^{2-} substitutes OH^- and PO_4^{3-}) [1,2]. CHA could be synthesized through wet chemical methods [2] and solid-state reactions [3]. Some researchers prefer using solid-state reactions such as mechanical milling because they are simple, inexpensive, and do not require additional treatments like product purification [3,4].

This study prepared B-type CHA from Indonesian limestone-based hydroxyapatite (HA) and magnesium carbonate ($MgCO_3$) as the precursors. Besides, as a CO_3^{2-} source, $MgCO_3$ will donate the Mg^{2+} to the synthetic CHA. Mg in the apatite component plays a vital role in bone metabolism, especially in stimulating osteoblast cell proliferation [3]. $MgCO_3$ was previously used as a precursor in synthesizing calcium phosphate by a wet chemical method [5]. However, no previous studies have used $MgCO_3$ as a precursor in synthesizing calcium phosphate by a dry-milling method. Additionally, the abundance of limestone in nature will support the availability of HA as a precursor. This work aims to synthesize CHA through dry mechano-milling between Indonesian limestone-based HA and $MgCO_3$.

2. Materials and methods

2.1. Sample preparation

CHA was synthesized through solid–solid reactions between HA and $MgCO_3$ by dry mechano-milling methods. Indonesian limestone-based HA was obtained from the previous study through wet precipitation methods [6], and $MgCO_3$ was purchased from Brataco Chemika were then mixed and milled at a weight ratio of HA and $MgCO_3$ of 6.67:1 in a planetary ball mill (Retsch PM 400, Germany) at 200 rpm. Alumina jar (500 ml) and alumina ball were used as milling media. The mass ratio between the sample and the milling ball was 1:2. The milling time interval of the samples varied from 1 to 8 h.

2.2. Characterization

The identification of crystalline phases of the samples was confirmed by X-ray diffraction (XRD, Bruker D8 Advance, Germany) at 40 kV and

* Corresponding authors at: Center for Ceramics, Ministry of Industry of Indonesia, Jalan Ahmad Yani 392, Bandung 40272, West Java, Indonesia (H. Damayanti). Material Science and Engineering Research Group, Faculty of Mechanical and Aerospace Engineering. Institut Teknologi Bandung, Indonesia. Jalan Ganesha 10, Bandung 40132, West Java, Indonesia (Lia A.T.W. Asri).
E-mail addresses: herlinadamayanti49@gmail.com (H. Damayanti), lia.asri@material.itb.ac.id (L.A.T.W. Asri).

https://doi.org/10.1016/j.matlet.2023.133999
Received 21 August 2022; Received in revised form 28 January 2023; Accepted 1 February 2023
Available online 3 February 2023

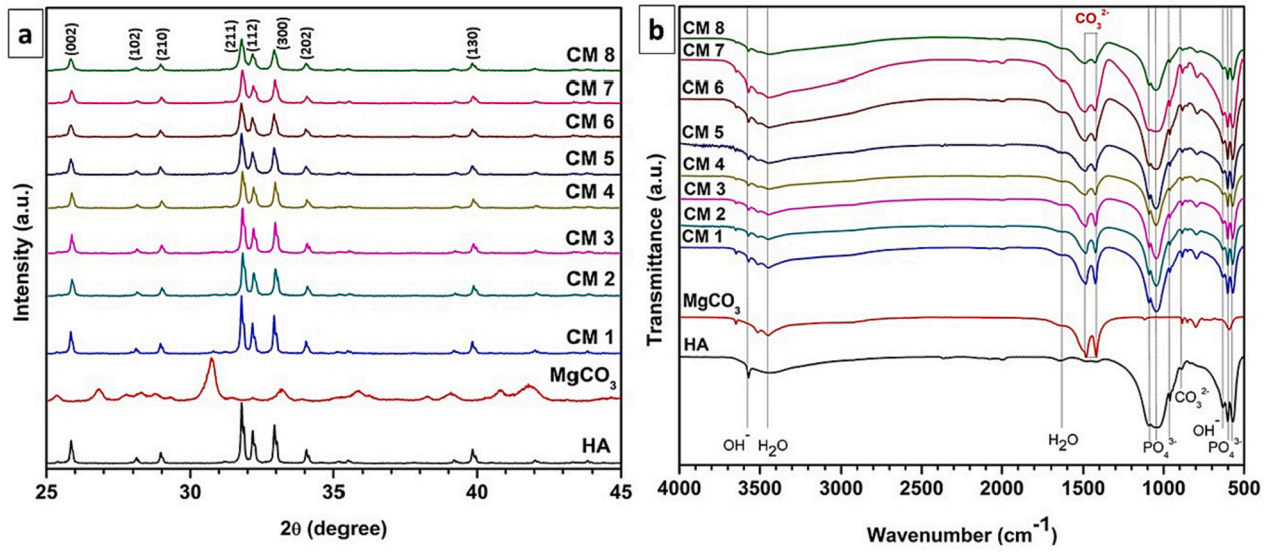

Fig. 1. (a) XRD patterns and (b) FTIR spectra of the precursors and dry-milled samples.

Table 1
Lattice Parameter, crystallite size, and particle size of HA and CHA.

Sample code	Interval Milling Time (hours)	$a = b$-axis (Å)	c-axis (Å)	c/a ratio	Crystalite size (nm)	Average particle size (μm)
HA	–	9.4241	6.8934	0.7315	12.7	2.87
CM 2	2	9.4002	6.8789	0.7318	7.8	2.43
CM 3	3	9.3976	6.8762	0.7317	7.9	2.39
CM 4	4	9.4003	6.8817	0.7321	7.1	2.48
CM 5	5	9.3955	6.8749	0.7317	6.5	2.54
CM 6	6	9.3913	6.8722	0.7318	6.2	2.85
CM 7	7	9.4064	6.8825	0.7317	6.3	2.59
CM 8	8	9.4047	6.8824	0.7318	7.8	2.75

40 mA with Cu/Kα (λ = 1.54060 Å) radiation source and scanned at the range of 10–90 (2θ) with a step size of 0.020. The chemical compositions were analyzed by X-ray fluorescence (XRF, Thermo Scientific ARL 9900, France). The infra-red spectra were collected using Fourier Transform Infra-Red (FT-IR, Bruker Alpha II, Germany). The surface morphologies were characterized using a scanning electron microscope (SEM, JEOL-JSM-IT300, Japan) at 20 kV. Particle size was measured by a laser diffraction particle size analyzer (Malvern Mastersizer 3000, UK).

3. Results and discussion

Fig. 1(a) shows the XRD patterns of precursors and synthesized material. CM 1 still showed characteristics peak of each precursor; HA appeared as the dominant phase and $MgCO_3$ peaks at 30.8° with low intensity. The increasing milling time resulted in the absence of $MgCO_3$ peaks as shown in Fig. S3 and S4. CM 2 indicates the start of the formation of CHA that is similar to and closely matches the standard pattern (JCPDS Card No: 09–0432) of HA with the highest peak at 2θ of 31.7° [7]. In CHA samples, broadening peaks indicate that the crystal lattice changes due to the substitution of CO_3^{2-} into the HA structure [7,8]. All diffraction peaks of CHA experience slight shifts compared to the initial HA substituting the Mg^{2+} ion to calcium sites at the HA matrix and can be integrated into the HA lattice [9]. Mg does not present as a second phase in the HA structure, thus allowing Mg to be only adsorbed on the surface of HA crystals [10]. The broadening and shifting peaks are presented in the supplementary data. Combining CO_3^{2-} and Mg^{2+} ions

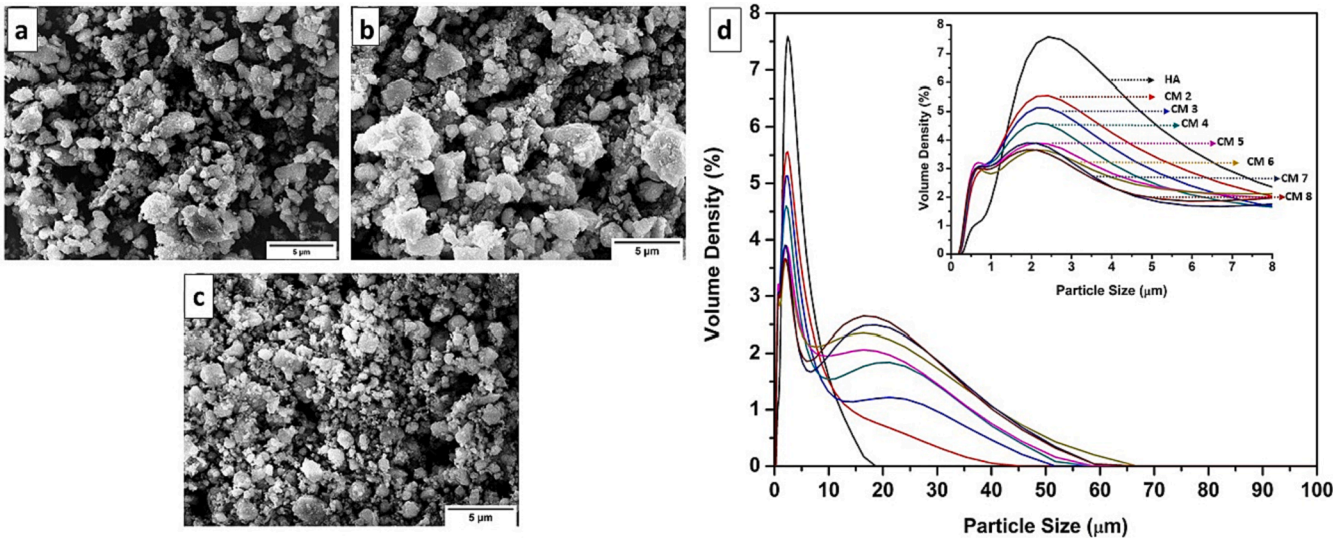

Fig. 2. SEM images of (a) HA, (b) CM 2, (c) CM 3, and (d) particle size distributions of the dry-milled CHA.

into the HA structure will change the lattice parameter shown in Table 1. Compared to HA, the a-axis and c-axis of all CHA samples decrease, but the ratio c/a parameter increases therefore exhibiting the substitution of PO_4^{3-} by CO_3^{2-} on the B-site. The obtained results corresponding to the work of M. Safarzadeh et al. and K. Benataya et al. [2,11] stated that unit cell dimensions of CHA are smaller than HA due to the CO_3 triangles being smaller than PO_4 tetrahedral. Likewise, the crystallite size decreases due to substituting CO_3^{2-} and Mg^{2+} into the HA structure through dry mechano-milling treatment, as shown in Table 1. The substitution of both ions will suppress the crystal growth of HA [2,8–10]. Thus, the formed CHA has a crystallite size smaller than pure HA. The XRF results show the calcium phosphate (Ca/P) atomic ratio of HA is 1.65 and increased in CHA, which is 1.66 for CM 2 and 1.73 for CM 8, which expected that CHA samples are non-stoichiometric apatite due to the substitution of CO_3^{2-} to PO_4^{3-} in the HA structure [2].

FTIR spectra (Fig. 1 (b)) exhibit the characteristic bands of PO_4^{3-} (1089–1092, 1044, 961, 601, and 567 cm^{-1}) and OH^- (632 and 3570 cm^{-1}) in the HA structure [12]. Absorption bands in the range 3000–3500 and 1647 cm^{-1} are assigned to the water molecule [10,13]. The characteristic bands of CO_3^{2-} at 885, 1424, and 1485 cm^{-1} indicate B-type CHA [2,11]. Fig. S6 shows the characteristic band of CO_3^{2-} residue from $MgCO_3$ at 800 cm^{-1}, which decreases with increasing milling time. It was also confirmed from the XRD results that the $MgCO_3$ peak was not present as the milling time increased. To conclude, FTIR and XRD results confirm the formation of B-type CHA.

SEM images in Fig. 2 (a-c) show the nearly spherical shape of HA and CHA particles agglomerated with the smallest particle size around 0.2 μm. Fig. 2 (d) demonstrates the dry-milled CHA particle size distribution with a size range of approximately 0.2–67 μm and confirms the smallest particle size of 0.2 μm by SEM. Fig. 2 and Table 1 illustrate the average particle size of CHA is ~ 2 μm with the decrease of volume density trend as an increase of the milling time.

4. Conclusions

B-type CHA containing Mg cations was synthesized through a dry mechano-milling of HA and $MgCO_3$. The ions of $MgCO_3$ have substituted HA structure to form the B-type of CHA with Mg trace element. The experimental results show that the increasing milling time affects the carbonate that enters the HA structure to form CHA. This research has proven to be developed further for biomaterial applications.

CRediT authorship contribution statement

Herlina Damayanti: Conceptualization, Investigation, Writing – original draft. **Karlina Noordiningsih:** Investigation. **Kristanto Wahyudi:** Conceptualization, Methodology. **Hernawan:** Resources. **Eneng Maryani:** Investigation, Writing – review & editing. **Anita Yuliati:** Supervision. **Devi Rianti:** Validation. **Lia A.T.W. Asri:** Supervision, Writing – review & editing. **Rifki Septawendar:** Conceptualization.

Declaration of Competing Interest

The authors declare that they have no known competing financial interests or personal relationships that could have appeared to influence the work reported in this paper.

Data availability

The data that has been used is confidential.

Acknowledgments

Authors thank The Indonesian Endowment Fund for Education (LPDP) for financial support, The Center for Ceramics in the Ministry of Industry of Indonesia, and the ITB Research Grant Program (PN-6-06-2022).

Appendix A. Supplementary data

Supplementary data to this article can be found online at https://doi.org/10.1016/j.matlet.2023.133999.

References

[1] P. Ptáček, Synthetic Phase with the Structure of Apatite, in: Chem. Apatites Their Synth. Analog. - Synth. Struct. Prop. Appl., INTECH, 2016: pp. 177–244. 10.5772/62212.
[2] M. Safarzadeh, S. Ramesh, C.Y. Tan, H. Chandran, Y.C. Ching, A.F.M. Noor, S. Krishnasamy, W.D. Teng, Sintering behaviour of carbonated hydroxyapatite prepared at different carbonate and phosphate ratios, Bol. La Soc. Esp. Ceram. y Vidr. 59 (2020) 73–80, https://doi.org/10.1016/j.bsecv.2019.08.001.
[3] S. Lala, M. Ghosh, P.K. Das, D. Das, T. Kar, S.K. Pradhan, Magnesium substitution in carbonated hydroxyapatite: Structural and microstructural characterization by Rietveld's refinement, Mater. Chem. Phys. 170 (2016) 319–329, https://doi.org/10.1016/j.matchemphys.2015.12.058.
[4] B. NasiriTabrizi, A. Fahami, R. EbrahimiKahrizsangi, F. Ebrahimi, New Frontiers in Mechanosynthesis: Hydroxyapatite – and Fluorapatite – Based Nanocomposite Powders, in: Nanocomposites New Trends Dev., INTECH, 2012: pp. 259–297. 10.5772/50160.
[5] W.L. Suchanek, K. Byrappa, P. Shuk, R.E. Riman, V.F. Janas, K.S. Tenhuisen, Mechanochemical-hydrothermal synthesis of calcium phosphate powders with coupled magnesium and carbonate substitution, J. Solid State Chem. 177 (2004) 793–799, https://doi.org/10.1016/j.jssc.2003.09.012.
[6] K. Wahyudi, H. Damayanti, R.J. Manullang, A. Ratnasari, Synthesis and phase transformation of hydroxyapatite from Indonesian natural sources Synthesis and Phase Transformation of Hydroxyapatite from Indonesian Natural Sources, AIP Conf. Proc. 020068 (2021), https://doi.org/10.1063/5.0051972.
[7] M. Safarzadeh, C.F. Chee, S. Ramesh, M.N.A. Fauzi, Effect of sintering temperature on the morphology, crystallinity and mechanical properties of carbonated hydroxyapatite (CHA), Ceram. Int. 46 (2020) 26784–26789, https://doi.org/10.1016/j.ceramint.2020.07.153.
[8] M. Wang, R. Qian, M. Bao, C. Gu, P. Zhu, Raman, FT-IR and XRD study of bovine bone mineral and carbonated apatites with different carbonate levels, Mater. Lett. 210 (2018) 203–206, https://doi.org/10.1016/j.matlet.2017.09.023.
[9] B. Gayathri, N. Muthukumarasamy, D. Velauthapillai, S.B. Santhosh, V. asokan,, Magnesium incorporated hydroxyapatite nanoparticles: Preparation, characterization, antibacterial and larvicidal activity, Arab. J. Chem. 11 (2018) 645–654, https://doi.org/10.1016/j.arabjc.2016.05.010.
[10] A. Farzadi, F. Bakhshi, M. Solati-Hashjin, M. Asadi-Eydivand, N.A.A. Osman, Magnesium incorporated hydroxyapatite: Synthesis and structural properties characterization, Ceram. Int. 40 (2014) 6021–6029, https://doi.org/10.1016/j.ceramint.2013.11.051.
[11] K. Benataya, M. Lakrat, L.L. Elansari, E. Mejdoubi, Synthesis of B-type carbonated hydroxyapatite by a new dissolution-precipitation method, Mater. Today Proc. 31 (2020) S83–S88. 10.1016/j.matpr.2020.06.100.
[12] N. Vargas-Becerril, D.A. Sánchez-Téllez, L. Zarazúa-Villalobos, D.M. González-García, M.A. Álvarez-Pérez, C. de León-Escobedo, L. Téllez-Jurado, Structure of biomimetic apatite grown on hydroxyapatite (HA), Ceram. Int. 46 (2020) 28806–28813, https://doi.org/10.1016/j.ceramint.2020.08.044.
[13] J.K. Abifarin, D.O. Obada, E.T. Dauda, D. Dodoo-Arhin, Experimental data on the characterization of hydroxyapatite synthesized from biowastes, Data Br. 26 (2019), 104485, https://doi.org/10.1016/j.dib.2019.104485.